Eur. Phys. J. B (2020) 93: 101
https://doi.org/10.1140/epjb/e2020-10122-6

THE EUROPEAN PHYSICAL JOURNAL B

Regular Article

Tailoring dipole effects for achieving thermal and electrical invisibility simultaneously

Liujun Xu[1,a], Xiongtao Zhao[2], Yupeng Zhang[2], and Jiping Huang[1,b]

[1] Department of Physics, State Key Laboratory of Surface Physics, and Key Laboratory of Micro and Nano Photonic Structures (MOE), Fudan University, Shanghai 200438, P.R. China
[2] Innovation & Research Institute of Hiwing Technology Academy, Beijing 100074, P.R. China

Received 9 March 2020 / Received in final form 24 April 2020
Published online 1 June 2020

Abstract. With the increasing requirement of metamaterials, integration and intellectualization have become the trends in order to enhance the manipulation efficiency of physical fields. Therefore, multiphysical functions and metamaterials have been proposed intensively. Meanwhile, the higher requirement of materials and structures is also put forward. In this work, by applying a shell and a dipole as two controllable conditions, multiphysical (say, thermal and electrical) invisibility can be obtained simultaneously with only common materials and simple structures. We explore the dipole effects in a core-shell structure and derive the requirements of the shell and dipole in both two and three dimensions, even considering the shells with material anisotropy. Finite-element simulations are consistent with theoretical analyses, confirming the feasibility of our scheme. These results may not only provide guidance to thermal and electrical management, but also benefit other physical fields such as electrostatics and magnetostatics.

1 Introduction

Since the proposal of transformation optics [1], transformation theories and metamaterials have made significant achievements in acoustic waves [2,3], matter waves [4], water waves [5,6], thermotics [7,8], fluid mechanics [9–11], dc current [12], caustics [13], etc. These studies consider only a single physical field. As the requirement of metamaterials goes up, it is found possible to manipulate multiphysical fields with a single device, thus realizing multiphysical functions and metamaterials. One classification of these multiphysical functions and metamaterials may depend on whether the multiphysical fields are coupled together. For decoupled fields, representative instances consider thermal and electrical fields [14–22], electromagnetic and acoustic waves [23–26], light and heat [27,28], etc. For coupled fields, typical examples are based on light-electrical effects [29,30], thermo-electric effects [31,32], conductive-convective effects [33–38], conductive-radiative effects [39–42], etc.

The feasibility of multiphysical functions and metamaterials mainly contributes to the similar dominant equations of multiphysical fields. However, an awkward situation is that there are few natural materials to meet the requirement. We take thermal and electrical fields as an example. If we expect to achieve multiphysical functions and metamaterials, the ratio between thermal and electrical conductivities should be the same in all regions [17], thus challenging natural materials. To solve the problem, one method is to apply the effective-medium theory [15,16], and another method is to combine passive and active schemes [19]. These two methods have a significant advantage in reducing the requirement of materials, but they still require complex structures. Therefore, there is still room for improving the method of multiphysical functions and metamaterials.

For this purpose, we study the dipole effects for achieving multiphysical invisibility. Here, multiphysical invisibility means that thermal and electrical gradients are both uniform in the matrix. The present scheme has no harsh requirement on materials and structures, which is beneficial to practical applications. The feasibility of our scheme lies in the particular field of a dipole which can just cancel the scattering of a core-shell structure. Essentially, we provide two controllable conditions (say, a shell and a dipole) to achieve multiphysical invisibility, so the requirement of materials and structures is naturally reduced.

2 Theory

We start from two dimensions (see Fig. 1) and consider a core-shell structure with core radius r_c and shell radius r_s embedded in a matrix. The subscripts c and s represent the core and shell, respectively. Since multiphysical

[a] e-mail: 13307110076@fudan.edu.cn
[b] e-mail: jphuang@fudan.edu.cn

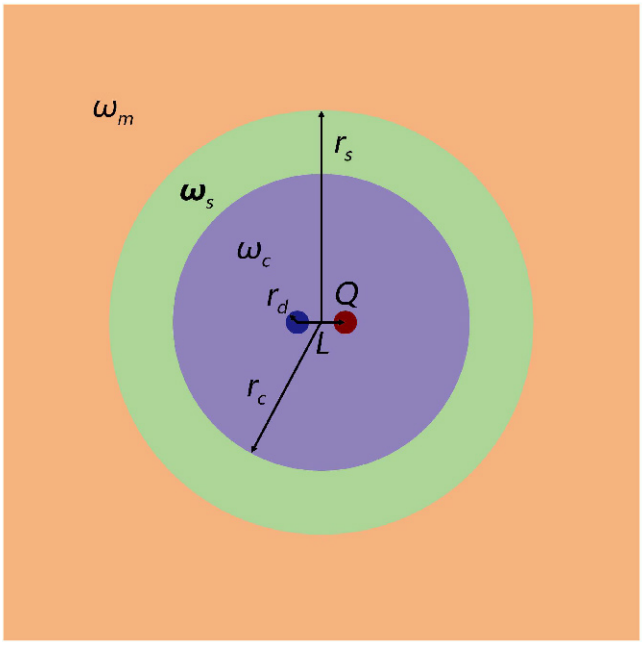

Fig. 1. Schematic diagram of our scheme.

fields refer to a thermal field and an electrical field, for the convenience of discussion, we use subscripts t and e to represent thermal parameters and electrical parameters, respectively. Then, the thermal (or electrical) conductivities of the core, shell, and matrix can be denoted as ω_{tc} (or ω_{ec}), $\boldsymbol{\omega}_{ts}$ (or $\boldsymbol{\omega}_{es}$), and ω_{tm} (or ω_{em}), respectively. Here, we consider only an anisotropic shell whose tensorial thermal and electrical conductivities can be expressed in cylindrical coordinates $(r,\,\theta)$ as $\boldsymbol{\omega}_{ts} = \mathrm{diag}\left(\omega_{ts}^{rr},\,\omega_{ts}^{\theta\theta}\right)$ and $\boldsymbol{\omega}_{es} = \mathrm{diag}\left(\omega_{es}^{rr},\,\omega_{es}^{\theta\theta}\right)$, respectively. We suppose that there are a thermal dipole and an electrical dipole in the center with dipole moments $P_t = Q_t L$ and $P_e = Q_e L$, respectively. Q_t and Q_e denote thermal power and electrical charge, respectively. L represents the distance between the two circular sources with radius r_d. Temperature and voltage are denoted as Ω_t and Ω_e, respectively. If a parameter has no subscripts t and e, it has multiphysical meanings. Then, the dominant equation of multiphysical processes can be generalized as

$$\boldsymbol{\nabla}\cdot\left(-\boldsymbol{\omega}\cdot\boldsymbol{\nabla}\Omega\right) = 0. \tag{1}$$

The multiphysical profiles in the core Ω_c, shell Ω_s, and matrix Ω_m can be expressed as [43]

$$\begin{aligned}\Omega_c &= \left(A_1 r + A_2 r^{-1}\right)\cos\theta,\\ \Omega_s &= \left(A_3 r^{u_1} + A_4 r^{u_2}\right)\cos\theta,\\ \Omega_m &= \left(A_5 r + A_6 r^{-1}\right)\cos\theta,\end{aligned} \tag{2}$$

where $u_{1,\,2} = \pm\sqrt{\omega_s^{\theta\theta}/\omega_s^{rr}}$. A_1, A_2, A_3, A_4, A_5, and A_6 are six coefficients to be determined. Among them, A_2 and A_5 can be determined by two limit analyses, respectively. The existence of A_2 results from the dipole effects, so we can obtain $A_2 = P/\left(2\pi\omega_c\right)$ which is exactly the profile of a dipole in an infinite core [44]. This expression of $A_2 = P/\left(2\pi\omega_c\right)$ is applicable when the distance between the hot and cold sources L is small enough. The smaller the distance L is, the better the performance is. Meanwhile, the radius of the hot and cold sources r_d does not affect the accuracy of A_2. When considering the profiles at infinity, we can obtain uniform fields, thus yielding $A_5 = G$ with $\boldsymbol{G} = -G\hat{\boldsymbol{x}}$ representing uniform fields. The rest four coefficients can be determined by the continuous potentials and fluxes on the boundaries, namely

$$\begin{aligned}\Omega_c\left(r = r_c\right) &= \Omega_s\left(r = r_c\right),\\ \Omega_s\left(r = r_s\right) &= \Omega_m\left(r = r_s\right),\\ -\omega_c\partial\Omega_c/\partial r\left(r = r_c\right) &= -\omega_s^{rr}\partial\Omega_s/\partial r\left(r = r_c\right),\\ -\omega_s^{rr}\partial\Omega_s/\partial r\left(r = r_s\right) &= -\omega_m\partial\Omega_m/\partial r\left(r = r_s\right).\end{aligned} \tag{3}$$

When $A_6 = 0$, the multiphysical profiles in the matrix are uniform, thus achieving multiphysical invisibility. Therefore, the dipole moments can be derived by solving equation (3) with $A_6 = 0$,

$$\begin{aligned}P = \Big[&r_c^{1+u_1} r_s^{1-u_1}\left(\omega_c - u_1\omega_s^{rr}\right)\left(-u_2\omega_s^{rr} + \omega_m\right)\\ &+ r_c^{1+u_2} r_s^{1-u_2}\left(\omega_c - u_2\omega_s^{rr}\right)\left(u_1\omega_s^{rr} - \omega_m\right)\Big]\frac{\pi G}{\left(u_1 - u_2\right)\omega_s^{rr}}.\end{aligned} \tag{4}$$

Now, we have two methods to achieve invisibility, say, a shell and a dipole. If a shell can just obtain thermal invisibility, a thermal dipole is not required ($P_t = 0$). However, such a shell cannot necessarily obtain electrical invisibility simultaneously, so an electrical dipole is required ($P_e \neq 0$). Conversely, if a shell can just obtain electrical invisibility, an electrical dipole is not required ($P_e = 0$). In this case, a thermal dipole is required ($P_t \neq 0$). The requirement to obtain a zero dipole moment ($P = 0$) is

$$\omega_m = \omega_s^{rr}\frac{u_1\left(\omega_c - u_2\omega_s^{rr}\right) - u_2\left(\omega_c - u_1\omega_s^{rr}\right) f^{(u_1-u_2)/2}}{\left(\omega_c - u_2\omega_s^{rr}\right) - \left(\omega_c - u_1\omega_s^{rr}\right) f^{(u_1-u_2)/2}}, \tag{5}$$

where $f = \left(r_c/r_s\right)^2$. So far, we have revealed the dipole effects for achieving multiphysical invisibility in two dimensions. The key to our scheme is to provide another controllable method (say, a dipole) beyond a shell. In this way, we can break the strict restriction of materials and structures, and achieve multiphysical invisibility.

On the same footing, we consider a three-dimensional case with an anisotropic shell in the spherical coordinates $(r,\,\theta,\,\varphi)$ which is expressed as $\boldsymbol{\omega}_s = \mathrm{diag}\left(\omega_s^{rr},\,\omega_s^{\theta\theta},\,\omega_s^{\varphi\varphi}\right)$ with $\omega_s^{\theta\theta} = \omega_s^{\varphi\varphi}$ for brevity. Then, the three-dimensional multiphysical profiles in the core Ω_c, shell Ω_s, and matrix Ω_m can be expressed as [43]

$$\begin{aligned}\Omega_c &= \left(A_1 r + A_2 r^{-2}\right)\cos\theta,\\ \Omega_s &= \left(A_3 r^{v_1} + A_4 r^{v_2}\right)\cos\theta,\\ \Omega_m &= \left(A_5 r + A_6 r^{-2}\right)\cos\theta,\end{aligned} \tag{6}$$

where $v_{1,\,2} = -1/2 \pm \sqrt{1/4 + 2\omega_s^{\theta\theta}/\omega_s^{rr}}$. A_1, A_2, A_3, A_4, A_5, and A_6 are six coefficients to be determined. With limit analyses similar to two dimensions, we can obtain

$A_2 = P/(4\pi\omega_c)$ [44] and $A_6 = G$. The rest four coefficients can also be determined by equation (3). By setting $A_6 = 0$, we can derive the dipole moments

$$P = \left[r_c^{2+v_1} r_s^{1-v_1} (\omega_c - v_1\omega_s^{rr})(-v_2\omega_s^{rr} + \omega_m) + r_c^{2+v_2} r_s^{1-v_2} (\omega_c - v_2\omega_s^{rr})(v_1\omega_s^{rr} - \omega_m)\right] \frac{4\pi G}{3(v_1 - v_2)\omega_s^{rr}}. \quad (7)$$

The requirement of a zero dipole moment ($P = 0$) is

$$\omega_m = \omega_s^{rr} \frac{v_1(\omega_c - v_2\omega_s^{rr}) - v_2(\omega_c - v_1\omega_s^{rr}) f^{(v_1 - v_2)/3}}{(\omega_c - v_2\omega_s^{rr}) - (\omega_c - v_1\omega_s^{rr}) f^{(v_1 - v_2)/3}}, \quad (8)$$

where $f = (r_c/r_s)^3$. Therefore, the dipole effects can help to achieve multiphysical invisibility in both two and three dimensions.

3 Finite-element simulations

We perform finite-element simulations with COMSOL MULTIPHYSICS (http://www.comsol.com/) to confirm our scheme. Firstly, we discuss a two-dimensional case with practical materials and apply horizontal multiphysical fields (see Fig. 2). For this purpose, the left and right boundaries are set at high and low temperatures/voltages, respectively. The top and bottom boundaries are thermally and electrically insulated. When a copper (Cu) core is embedded in an aluminum (Al) matrix, the isothermal and isopotential lines are repelled because the parameters of Cu and Al do not match (see Figs. 2a and 2b). Therefore, the core is visible with an in-plane detection. To remove the distortions of isolines, we wrap up the core with a shell made of magnesium (Mg) alloy. By designing a thermally-matched radius according to equation (5), we can obtain thermal invisibility because the thermal dipole moment with this radius is zero (see Fig. 2c). Unfortunately, such a radius is not electrically matched, so the isopotential lines are still distorted (see Fig. 2d). Then, we place an electrical dipole designed with equation (4) in the center, and the isopotential lines become undistorted (see Fig. 2e). Therefore, we achieve multiphysical invisibility with a shell and an electrical dipole. Certainly, we can also design an electrically-matched radius according to equation (5) to achieve electrical invisibility (see Fig. 2g). However, such a radius is not thermally matched, so only a shell cannot achieve thermal invisibility (see Fig. 2f). Then, we place a thermal dipole designed with equation (4) in the center, and the isothermal lines become undistorted (see Fig. 2h). Therefore, we can also achieve multiphysical invisibility with a shell and a thermal dipole.

For quantitative analyses, we plot the data at $x = -8$ cm of each simulation in Figure 2 (see Fig. 3). The temperature and voltage distributions are presented in Figures 3a and 3b, respectively. Clearly, the profiles of Figures 2c, 2h, 2e, and 2g are uniform, thus achieving multiphysical invisibility.

The shell applied in Figure 2 is isotropic. We further discuss an anisotropic shell (see Fig. 4). Similar to two

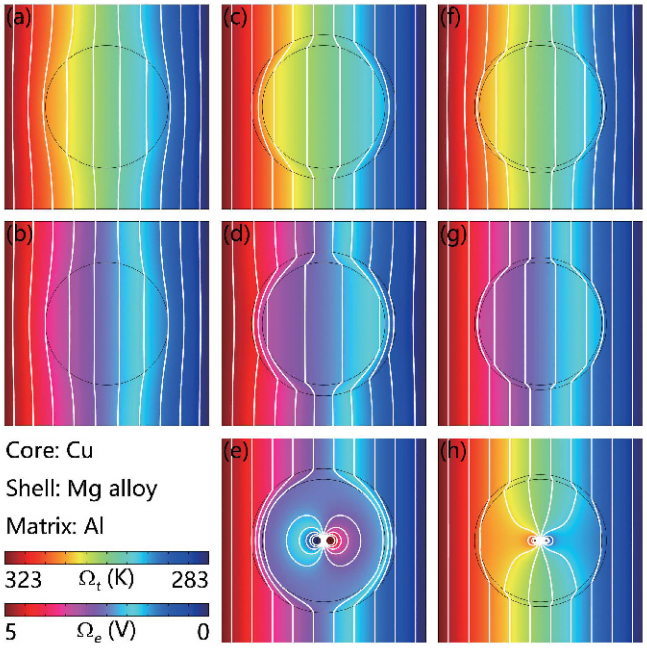

Fig. 2. Two-dimensional case with isotropic shells. Rainbow color maps represent temperature distributions, and disco color maps represent voltage distributions. White lines represent isolines. The core, shell, and matrix are copper, magnesium alloy, and aluminum, respectively. Copper: $\omega_t = 400$ W m^{-1} K^{-1}, $\omega_e = 5.9 \times 10^7$ S m^{-1}; Magnesium alloy: $\omega_t = 73$ W m^{-1} K^{-1}, $\omega_e = 0.7 \times 10^7$ S m^{-1}; Aluminum: $\omega_t = 220$ W m^{-1} K^{-1}, $\omega_e = 3.7 \times 10^7$ S m^{-1}. (a) and (b) Only a core with radius $r_c = 6$ cm embedded in a matrix with size 20×20 cm^2. (c)–(e) A shell with radius $r_s = 7$ cm surrounded the core. (e) An electrical dipole with $P_e = 8.9 \times 10^6$ C m, $L = 1$ cm, and $r_d = 0.2$ cm in the center. (f)–(h) A shell with radius $r_s = 6.4$ cm surrounded the core. (h) A thermal dipole with $P_t = -239.6$ W m and the same size as (e) in the center.

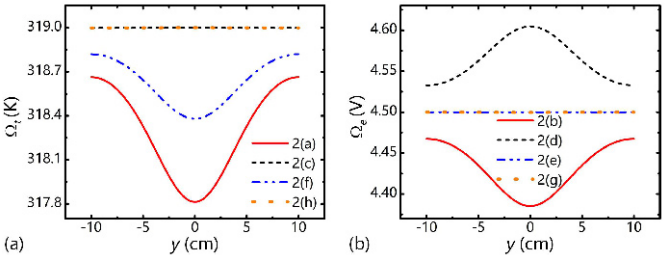

Fig. 3. Quantitative analyses of Figure 2. Temperature and voltage distributions at $x = -8$ cm (the origin is located in the center of each simulation) are plotted in (a) and (b), respectively. Each line corresponds to a figure shown in the legend.

dimensions, when a core composed of Mg alloy is embedded in an Al matrix, the isothermal and isopotential lines are contracted (see Figs. 4a and 4b). With a thermally-matched anisotropic shell designed with equation (5), we can achieve thermal invisibility without a thermal dipole (see Fig. 4c) and obtain electrical invisibility with this shell and an electrical dipole designed with equation (4)

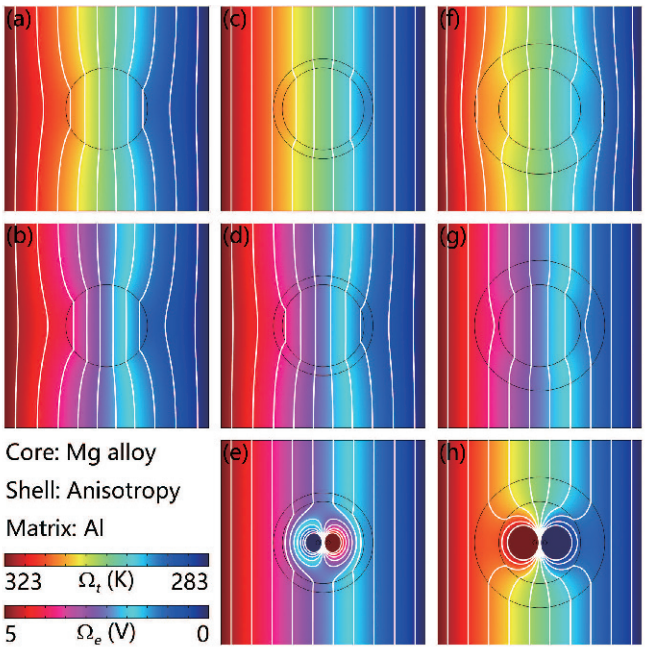

Fig. 4. Two-dimensional case with anisotropic shells. The core and matrix are magnesium alloy and aluminum, respectively. The shell has a tensorial thermal conductivity $\boldsymbol{\omega}_t = \text{diag}\,(400, 800)$ W m^{-1} K^{-1} and a tensorial electrical conductivity $\boldsymbol{\omega}_e = \text{diag}\,(4, 8) \times 10^7$ S m^{-1}. The core in (a)–(h) has a radius of $r_c = 4$ cm. The shell in (c)–(e) has a radius of $r_s = 4.9$ cm, and that in (f)–(h) has a radius of $r_s = 6.4$ cm. The electrical dipole in (e) has a dipole moment of $P_e = 2.5 \times 10^6$ C m with $L = 1$ cm and $r_d = 0.2$ cm, and the thermal dipole in (h) has a dipole moment $P_t = -319.6$ W m with the same size as (e).

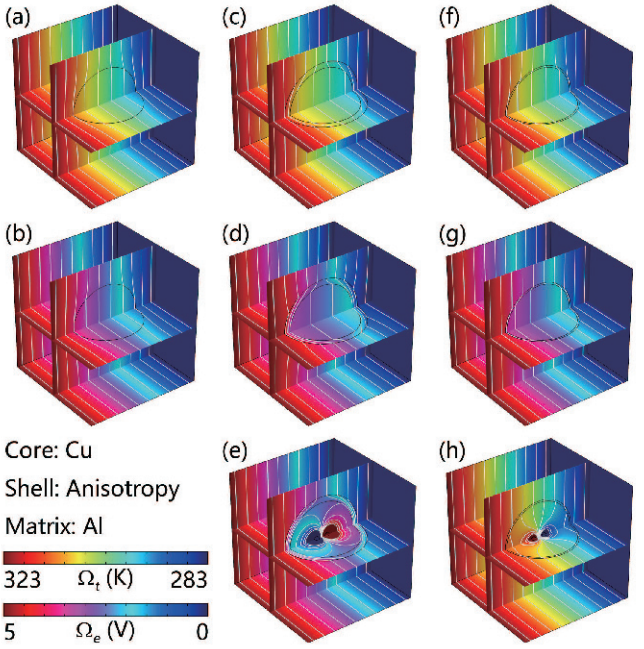

Fig. 5. Three-dimensional case ($20 \times 20 \times 20$ cm^3) with anisotropic shells. The core and matrix are copper and aluminum, respectively. The shell has a tensorial thermal conductivity $\boldsymbol{\omega}_t = \text{diag}\,(80, 120, 120)$ W m^{-1} K^{-1} and a tensorial electrical conductivity $\boldsymbol{\omega}_e = \text{diag}\,(0.5, 1, 1) \times 10^7$ S m^{-1}. The core in (a)–(h) has a radius of $r_c = 6$ cm. The shell in (c)–(e) has a radius of $r_s = 7$ cm, and that in (f)–(h) has a radius of $r_s = 6.3$ cm. The electrical dipole in (e) has a dipole moment of $P_e = 1.5 \times 10^6$ C m with $L = 2$ cm and $r_d = 0.4$ cm, and the thermal dipole in (h) has a dipole moment $P_t = -24.3$ W m with the same size as (e).

(see Figs. 4d and 4e). We can also design an electrically-matched anisotropic shell according to equation (5), and achieve electrical invisibility without an electrical dipole (see Fig. 4g). In this case, thermal invisibility cannot be obtained (see Fig. 4f), and a thermal dipole designed with equation (4) can help to achieve thermal invisibility (see Fig. 4h).

Finally, we consider a three-dimensional case with a Cu core embedded in an Al matrix (see Figs. 5a and 5b). With a thermally-matched anisotropic shell designed with equation (8) and an electrical dipole designed with equation (7), three-dimensional multiphysical invisibility can be achieved (see Figs. 5c–5e). Certainly, multiphysical invisibility can also be obtained with an electrically-matched anisotropic shell designed with equation (8) and a thermal dipole designed with equation (7) (see Figs. 5f–5h).

4 Discussions

For practical applications, thermal dipoles can be achieved with ceramic heaters and peltier coolers, and electrical dipoles can be realized with constant-power sources. So, our scheme is not difficult to be confirmed by experiments. Although multiphysical invisibility in this work refers to thermal and electrical invisibility, such a concept can also be extended to other physical fields such as electrostatics [45,46] and magnetostatics [47] where the realization of dipoles is mature. Furthermore, the dipole effects are also promising to be applied in other systems beyond core-shell structures such as many-particle systems [48–50], and may be extended to transient states by take time-dependent dipole moments into consideration. Nevertheless, there is only an analytical solution to circular/spherical cases, but one may extend these results to irregular shapes by applying the method of topology optimization [51–54].

5 Conclusions

In summary, we have fully discussed the dipole effects to achieve multiphysical invisibility, and derive the requirements of a shell and a dipole in both two and three dimensions. Meanwhile, we also discuss the requirement of a zero dipole moment and the cases with material anisotropy. These theoretical analyses are confirmed by finite-element simulations, indicating the feasibility of our scheme. Furthermore, our scheme has desirable features such as simple structure, material insensitivity, flexible manipulation, etc. Therefore, broad applications

can be expected in realizing intelligent camouflage and illusion [55–66].

We acknowledge the financial support by the National Natural Science Foundation of China under Grant No. 11725521.

Author contribution statement

L.X. and J.H. designed research; L.X., X.Z., and Y.Z. performed research and analyzed data; and L.X., X.Z., Y.Z., and J.H. wrote the paper.

References

1. J.B. Pendry, D. Schurig, D.R. Smith, Science **312**, 1780 (2006)
2. S.A. Cummer, D. Schurig, New J. Phys. **9**, 45 (2007)
3. H.Y. Chen, C.T. Chan, Appl. Phys. Lett. **91**, 183518 (2007)
4. S. Zhang, D.A. Genov, C. Sun, X. Zhang, Phys. Rev. Lett. **100**, 123002 (2008)
5. C.Y. Li, L. Xu, L.L. Zhu, S.Y. Zou, Q.H. Liu, Z.Y. Wang, H.Y. Chen, Phys. Rev. Lett. **121**, 104501 (2018)
6. S.Y. Zou, Y.D. Xu, R. Zatianina, C.Y. Li, X. Liang, L.L. Zhu, Y.Q. Zhang, G.H. Liu, Q.H. Liu, H.Y. Chen, Z.Y. Wang, Phys. Rev. Lett. **123**, 074501 (2019)
7. C.Z. Fan, Y. Gao, J.P. Huang, Appl. Phys. Lett. **92**, 251907 (2008)
8. T.Y. Chen, C.N. Weng, J.S. Chen, Appl. Phys. Lett. **93**, 114103 (2008)
9. Y.A. Urzhumov, D.R. Smith, Phys. Rev. Lett. **107**, 074501 (2011)
10. J. Park, J.R. Youn, Y.S. Song, Phys. Rev. Lett. **123**, 074502 (2019)
11. J. Park, J.R. Youn, Y.S. Song, Phys. Rev. Appl. **12**, 061002 (2019)
12. F. Yang, Z.L. Mei, T.Y. Jin, T.J. Cui, Phys. Rev. Lett. **109**, 053902 (2012)
13. H.Y. Peng, H.Y. Chen, Phys. Rev. Appl. **12**, 064030 (2019)
14. J.Y. Li, Y. Gao, J.P. Huang, J. Appl. Phys. **108**, 074504 (2010)
15. M. Moccia, G. Castaldi, S. Savo, Y. Sato, V. Galdi, Phys. Rev. X **4**, 021025 (2014)
16. Y.G. Ma, Y.C. Liu, M. Raza, Y.D. Wang, S.L. He, Phys. Rev. Lett. **113**, 205501 (2014)
17. T.Z. Yang, X. Bai, D.L. Gao, L.Z. Wu, B.W. Li, J.T.L. Thong, C.W. Qiu, Adv. Mater. **27**, 7752 (2015)
18. C.W. Lan, B. Li, J. Zhou, Opt. Express **23**, 24475 (2015)
19. C.W. Lan, K. Bi, Z.H. Gao, B. Li, J. Zhou, Appl. Phys. Lett. **109**, 201903 (2016)
20. C.W. Lan, K. Bi, X.J. Fu, B. Li, J. Zhou, Opt. Express **24**, 23072 (2016)
21. L. Zhang, Y. Shi, Opt. Mater. Express **8**, 2600 (2018)
22. G.Q. Xu, X. Zhou, H.C. Zhang, H.P. Tan, Energy Convers. Manage. **187**, 546 (2019)
23. Y.H. Yang, H.P. Wang, F.X. Yu, Z.W. Xu, H.S. Chen, Sci. Rep. **6**, 20219 (2016)
24. G.Y. Song, C. Zhang, Q. Cheng, Y. Jing, C.W. Qiu, T.J. Cui, Opt. Express **26**, 22916 (2018)
25. C. Zhang, W.K. Cao, J. Yang, J.C. Ke, M.Z. Chen, L.T. Wu, Q. Cheng, T.J. Cui, ACS Appl. Mater. Interfaces **11**, 17050 (2019)
26. F. Sun, Y.C. Liu, S.L. He, Opt. Express **28**, 94 (2020)
27. W.K.P. Barros, E. Pereira, Sci. Rep. **8**, 11453 (2018)
28. Z.Y. Zhou, X.Y. Shen, C.C. Fang, J.P. Huang, ES Energy Environ. **6**, 85 (2019)
29. W.X. Jiang, C.Y. Luo, S. Ge, C.W Qiu, T.J. Cui, Adv. Mater. **27**, 4628 (2015)
30. T.C. Han, Y.X. Liu, L. Liu, J. Qin, Y. Li, J.Y. Bao, D.Y. Ni, C.W. Qiu, Sci. Rep. **8**, 12208 (2018)
31. T. Stedman, L.M. Woods, Sci. Rep. **7**, 6988 (2017)
32. S.Y. Huang, J.W. Zhang, M. Wang, W. Lan, R. Hu, X.B. Luo, ES Energy Environ. **6**, 51 (2019)
33. D. Torrent, O. Poncelet, J.C. Batsale, Phys. Rev. Lett. **120**, 125501 (2018)
34. G.L. Dai, J. Shang, J.P. Huang, Phys. Rev. E **97**, 022129 (2018)
35. Y. Li, K.J. Zhu, Y.G. Peng, W. Li, T.Z. Yang, H.X. Xu, H. Chen, X.F. Zhu, S.H. Fan, C.W. Qiu, Nat. Mater. **18**, 48 (2019)
36. Y. Li, Y.G. Peng, L. Han, M.A. Miri, W. Li, M. Xiao, X.F. Zhu, J.L. Zhao, A. Alu, S.H. Fan, C.W. Qiu, Science **364**, 170 (2019)
37. F.B. Yang, L.J. Xu, J.P. Huang, ES Energy Environ. **6**, 45 (2019)
38. L.J. Xu, J.P. Huang, Sci. China Phys. Mech. Astron. **63**, 228711 (2020)
39. Y. Li, X. Bai, T.Z. Yang, H. Luo, C.W. Qiu, Nat. Commun. **9**, 273 (2018)
40. L.J. Xu, J.P. Huang, Phys. Rev. Appl. **12**, 044048 (2019)
41. L.J. Xu, G.L. Dai, J.P. Huang, Phys. Rev. Appl. **13**, 024063 (2020)
42. J.L. Song, S.Y. Huang, Y.P. Ma, Q. Cheng, R. Hu, X.B. Luo, Opt. Express **28**, 875 (2020)
43. L.J. Xu, S. Yang, J.P. Huang, Phys. Rev. E **99**, 022107 (2019)
44. L.J. Xu, S. Yang, J.P. Huang, Phys. Rev. E **100**, 062108 (2019)
45. G.W. Milton, N.A.P. Nicorovici, Proc. R. Soc. A **462**, 3027 (2006)
46. L.J. Xu, J.P. Huang, Eur. Phys. J. B **92**, 53 (2019)
47. X. Dai, J.C. Jiang, AIP Adv. **10**, 025211 (2020)
48. L.J. Xu, S. Yang, J.P. Huang, Phys. Rev. Appl. **11**, 034056 (2019)
49. G.L. Dai, J.P. Huang, Int. J. Heat Mass Transfer **147**, 118917 (2019)
50. L.J. Xu, S. Yang, J.P. Huang, Eur. Phys. J. B **92**, 264 (2019)
51. G. Fujii, Y. Akimoto, M. Takahashi, Appl. Phys. Lett. **112**, 061108 (2018)
52. G. Fujii, Y. Akimoto, M. Takahashi, J. Appl. Phys. **123**, 233102 (2018)
53. G. Fujii, Y. Akimoto, Appl. Phys. Lett. **115**, 174101 (2019)
54. G. Fujii, Y. Akimoto, Int. J. Heat Mass Transfer **137**, 1312 (2019)
55. T.C. Han, X. Bai, J.T.L. Thong, B.W. Li, C.W. Qiu, Adv. Mater. **26**, 1731 (2014)
56. Y.X. Liu, W.L. Guo, T.C. Han, Int. J. Heat Mass Transfer **115**, 1 (2017)

57. T.C. Han, P. Yang, Y. Li, D.Y. Lei, B.W. Li, K. Hippalgaonkar, C.W. Qiu, Adv. Mater. **30**, 1804019 (2018)
58. R. Hu, S.L. Zhou, Y. Li, D.Y. Lei, X.B. Luo, C.W. Qiu, Adv. Mater. **30**, 1707237 (2018)
59. S.L. Zhou, R. Hu, X.B. Luo, Int. J. Heat Mass Transfer **127**, 607 (2018)
60. J. Guo, Z.G. Qu, Int. J. Heat Mass Transfer **127**, 1212 (2018)
61. R. Hu, S.Y. Huang, M. Wang, L.L. Zhou, X.Y. Peng, X.B. Luo, Phys. Rev. Appl. **10**, 054032 (2018)
62. L.J. Xu, C.R. Jiang, J.P. Huang, Eur. Phys. J. B **91**, 166 (2018)
63. R. Hu, S.Y. Huang, M. Wang, X.L. Luo, J. Shiomi, C.W. Qiu, Adv. Mater. **31**, 1807849 (2019)
64. X.Y. Peng, R. Hu, ES Energy Environ. **6**, 39 (2019)
65. J. Qin, W. Luo, P. Yang, B. Wang, T. Deng, T.C. Han, Int. J. Heat Mass Transfer **141**, 487 (2019)
66. G.Q. Xu, X. Zhou, J.Y. Zhang, Int. J. Heat Mass Transfer **142**, 118434 (2019)